On-chip collection of particles and cells by AC electroosmotic pumping and dielectrophoresis using asymmetric microelectrodes

Elizabeth M. Melvin,[1] Brandon R. Moore,[1] Kristin H. Gilchrist,[2] Sonia Grego,[2] and Orlin D. Velev[1,a)]
[1]*Department of Chemical and Biomolecular Engineering, North Carolina State University, Raleigh, North Carolina 27695-7905, USA*
[2]*RTI International, Research Triangle Park, North Carolina 27709-2194, USA*

(Received 7 May 2011; accepted 12 July 2011; published online 10 August 2011)

The recent development of microfluidic "lab on a chip" devices requiring sample sizes <100 μL has given rise to the need to concentrate dilute samples and trap analytes, especially for surface-based detection techniques. We demonstrate a particle collection device capable of concentrating micron-sized particles in a predetermined area by combining AC electroosmosis (ACEO) and dielectrophoresis (DEP). The planar asymmetric electrode pattern uses ACEO pumping to induce equal, quadrilateral flow directed towards a stagnant region in the center of the device. A number of system parameters affecting particle collection efficiency were investigated including electrode and gap width, chamber height, applied potential and frequency, and number of repeating electrode pairs and electrode geometry. The robustness of the on-chip collection design was evaluated against varying electrolyte concentrations, particle types, and particle sizes. These devices are amenable to integration with a variety of detection techniques such as optical evanescent waveguide sensing. © *2011 American Institute of Physics*. [doi:10.1063/1.3620419]

I. INTRODUCTION

Lab-on-a-chip or micro total analysis systems (μTAS) offer great potential and numerous advantages over conventional benchtop techniques for biological analysis including reduced sample size, lowered possibility for contamination, decreased waste, and reduced size of the analytical equipment. Recently, research has been focused not only on streamlining the steps of sample preparation and analysis, but also on combining sample preparation and analysis in a single device. In doing so, μTAS devices are, in many cases, more efficient and can achieve detection more rapidly than their macro-scale laboratory counterparts.

A common complication with the use of μTAS devices for biological detection in samples of less than 100 μL is the need to pre-concentrate the analyte. The analyte in the samples, especially particulates of biological origin, may be very dilute, invoking the need to collect enough particles and direct them to a detection area. The typical microfluidic devices require cells or other analytes to be physically bound or brought close to the surface of a particular transducer to increase the accuracy of detection. Surface-bound microfluidic devices have been successfully coupled with chemical[1–5] and optical[6–13] transducers to rapidly detect cells and particles in microliter suspensions. However, in order to achieve rapid detection, the time for establishing diffusion equilibrium of the analyte to the transducer should be kept to a minimum, requiring small fluidic chamber heights and, consequently, small sample volumes. The analyte should also bind to the transducer surface rapidly and with a high affinity.

A large portion of methods for particulate collection is based on electric fields. Microfabricated electrodes have been extensively used to manipulate analytes using AC fields and can be

a)Author to whom correspondence should be addressed. Electronic mail: odvelev@ncsu.edu.

easily integrated with microfludic devices. When an AC electric field is applied to a suspension of particles in an electrolyte solution, the particles and the medium are subjected to AC electric field-induced forces such as dielectrophoresis (DEP) and AC electroosmosis (ACEO). DEP is the electrically induced movement of a particle based on its relative polarizability compared to the suspension media. When subjected to a non-uniform electric field, a particle becomes polarized and is drawn towards or away from the region penetrated by the electric field. Particles that are more polarizable than the suspension media are drawn toward the region of the highest electric field (positive DEP). Conversely, if a particle is less polarizable than the media, it is repelled from the region of the strongest electric field (negative DEP). The polarized particles also commonly form chains in the direction of the electric field. The dielectrophoretic force is dependent on the intensity of the electric field ($|E|$), the radius of the particle (r), and the effective permittivity of the particle in the media (ε_p, ε_m) (Eq. (1)),[14]

$$\langle F_{DEP} \rangle = \pi r^3 \varepsilon_m \mathrm{Re}\left[\frac{\varepsilon_p - \varepsilon_m}{\varepsilon_p + 2\varepsilon_m}\right] \nabla |E|^2. \tag{1}$$

The AC fields also induce fluid flows in some electrode configurations by ACEO. The motion is initiated by the additional ionic charges attracted by the field to the counterionic double layer.[14] A non-uniform electric field leads to fluid movement driven by the tangential electric field (E_t). The velocity of the fluid (u_x) is dependent on the potential drop across the double layer (ψ), the frequency of the electric field (ω) and the charge of the double layer (ε_1)[14]

$$\langle u_x \rangle = \frac{1}{2} \mathrm{Re}\left[\frac{\varepsilon_1 E_t \psi(\omega)}{\eta}\right]. \tag{2}$$

The fluid velocity in AC electroosmosis is potential and frequency dependent. AC electroosmosis usually occurs between the frequencies of 10 Hz and 10 kHz, while fluid flow occurring at higher frequencies is typically due to electrothermal effects.[14] Asymmetric electrode patterns have been shown to produce flows that can be used for microfluidic pumping.[15–24] Electrodes can be arranged on a substrate surface in such a way as to induce asymmetric electric field gradients at the electrodes, thereby generating a local and bulk liquid flow. The asymmetric field creates a vortex near the edge of the electrode, driving a bulk flow analogous to a conveyor belt. At applied potentials from 0.1 to 10 V, planar asymmetric electrodes have been used to produce flows that are capable of transporting particles.[17–19,21,22,25]

In this paper, we introduce a μTAS device using ACEO flow induced by co-planar asymmetric electrodes arranged in a "corral" configuration, exploited not only for pumping the liquid but for collecting particles in a target location on the device. Previously in our group, an ACEO corral device was used to collect particles and cells in the center of an energized electrode surrounded by a dielectric layer of an insulative photoresist.[26] The asymmetrical AC field induced AC electroosmotic flows at each edge of the dielectric photoresist that drove a bulk fluid flow towards the center of the square corral. Densely packed particles were collected via a particle front originating at the photoresist edge and migrating over time inward towards the center. Particle collection in this device required over 1 h, which may be too long for some practical applications. The present new configuration uses a quadrilateral arrangement of repeating asymmetrical electrodes surrounding a 1×1 mm collection region (Figure 1). All electrode segments surrounding the corral are simultaneously energized with AC fields, driving bulk fluid flow from each direction and collecting the particles within a centrally located stagnant region. A key advantage of this configuration is that it uses coplanar electrodes surrounding the collection area as opposed to our earlier patterned sandwich configuration. The new configuration is more efficient and compatible with evanescent wave sensing devices.[6–8,12,28] We report the characterization of this particle/cell collection device with regard to chamber height, applied potentials, frequency, electrode geometry, electrode and gap width, repetition of asymmetric electrode patterns, and electrolyte concentration. We also introduce techniques combining ACEO with DEP to improve the performance of the device for collecting particles and cells from suspension.

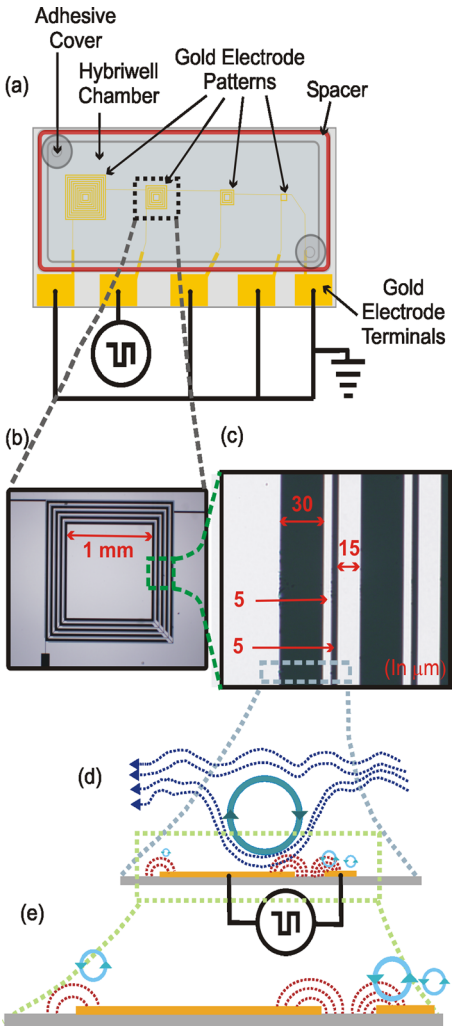

FIG. 1. (a) Top view of fully assembled planar electrode collection device. The square-wave AC current is applied to the magnified 5-repeat segment electrode design, while the others are grounded. (b) Micrograph of 5-repeat segment electrode design. The collection area is 1 mm for each electrode repeat patterns (1, 3, 5, 10 repeats). (c) Enlargement of electrode configuration with electrode dimensions in microns. The repeat segments, starting at the outermost edge, include a thin electrode followed by a 5 μm gap and a larger 30 μm electrode. Each segment is separated by a 15 μm gap. (d) Enlarged side view of planar electrodes on glass substrate and induced ACEO flow. The ACEO flow over the asymmetric electrodes is in the form of a large eddy induced just above the edge of the large electrode adjacent to the small gap. (e) Enlarged side view of small eddies formed just above the electrode surface [adapted from Ramos *et al.* (Ref. 27)].

II. METHODOLOGY

A. Sample preparation

Fluorescent 1 μm sulfate latex particles (Molecular Probes, Eugene, OR) were washed three times by agitation and centrifugation with deionized (DI) water from a Millipore RiOs purification system to remove any impurities and surfactants. The particles were diluted to 0.1 wt. % in DI water, 0.001 and 0.01 mM PBS, 10 mM PBS, or tap water. The conductivities of the DI water, PBS dilutions, and tap water were 0.25 μS/cm (DI water), 8.0 μS/cm (0.001 mM PBS), 36.0 μS/cm (0.01 mM PBS), 17.0 mS/cm (10 mM PBS), and 235 μS/cm (tap water). Yeast cell (Fleischmann's Ankenny, IA) samples were hydrated in DI water and were also washed by agitation and centrifugation to remove any residual proteins and sugars dried with the yeast cells during the manufacturing process. Yeast cell suspensions were diluted to 0.1 wt. % to compare with the latex particle dispersions.

B. Electrode chip fabrication

Gold-on-glass planar electrode chips were designed based on literature on ACEO and DEP particle collections.[15–24,26,27] (see Supplementary Material for design considerations[29]). The microelectrode devices were fabricated by Research Triangle Institute International using a single mask layer on 4 in., 700 μm thick borofloat glass wafers by a standard photolithographic lift-off process. Negative photoresist coated wafers (NFR016D2, 3.5 μm thick, JSR Micro, Inc. Sunnydale, CA) were UV exposed (Suss MicroTec MA8, Garching, Germany). Following a post-exposure bake, wafers were developed in PD523AD (JSR Micro, Inc. Sunnyvale, CA). Chromium (100 Å) and gold (1000 Å) were deposited by E-beam evaporation, followed by lift-off in N-Methyl-Pyrrolidinone (NMP) (JT Baker/Mallinckrod Chemicals, Phillipsburg, NJ). The wafers were cut to device size of 26×17 mm with a dicing saw. Each die consisted of 3-4 electrode corrals configurations with independently addressable contact pads and a common ground (Figure 1(a)).

C. Experimental apparatus and data acquisition

Electric wire leads were soldered to the electrode terminal pads of the devices. Fluidic chambers with depths of 250, 750, and 1600 μm were constructed with a 250 μm thick Grace Biolab Hybriwell chamber and a spacer of the designed thickness (Grace BioLabs Bend, OR) (Figure 1(a)). After loading approximately 80-250 μL of sample and evacuating bubbles, 3M adhesive seals were placed over the loading ports to prevent leakage and evaporation.

For each test, only one patterned electrode collection set was energized, while the other patterns were grounded. A 33120A Agilent function generator (Agilent Inc., Santa Clara, CA) was connected to the chip through a 4.7 μF capacitor (Radio Shack, Fort Worth, TX), selected to be large enough to filter the DC current component at all frequencies used without distorting the AC square wave signal. The potential was monitored using a GDM-8034 GW digital multimeter (Instek Inc., Chico, CA). The square wave AC voltage was set to 0.05–6 V at frequencies ranging from 10 Hz to 1 MHz. The crossover frequency for similar latex particles is on the order of 10^6 Hz,[14] so the ACEO effects were observed in conditions where the DEP, if present, would be positive.

The particle concentration processes were observed with an Olympus BX-61 microscope (Tokyo, Japan) at $4\times$, $10\times$, and $50\times$ magnifications. Time lapse images were collected every 10 s for a total of 15 min per trial. Relative particle velocities and changes in concentration density were analyzed from the digital images by using Adobe Photoshop software. The particle velocities were determined by measuring particle displacement by subtracting the coordinates measured frame to frame and dividing this displacement by the time elapsed. For the particle concentration density, the color micrographs were adjusted to 8-bit grayscale image. The average grayscale value of a 140 square-pixel area (5 pixels $\times$ 28 pixels) was evaluated at 25 μm increments starting from the electrode edge and ending at the collection area center. The analyzed region included particles and bare glass exclusively, eliminating electrodes, which appear black. The latex particles appear gray in the micrographs and, with increased particle density, the pixels darken and the grayscale values of the pixels decreased (255 is white). The gray value percent deviation from white (%DFW) was calculated by averaging the grayscale pixel color number for each point along the width of the collection area and normalizing it against the grayscale value from same area in the image at time $t = 0$.

III. RESULTS

The goal of this work is to collect the dispersed particles and concentrate them in dense deposit within a central 1 mm^2 collection region. This could allow to most effectively couple such a particle collection device with an evanescent optical wave guide or other type of detection or analysis device. Further, any practical handheld device necessitates rapid collection (under 15 min) at low applied potentials and frequencies. For simplicity, we used a singular mask photolithography process to create the quadrilateral concentric electrode pair patterns without overlaps. The 1×1 mm dimensions for the collection area were chosen to correspond to the minimum size of a typical optical waveguide grating.[6] Each electrode pair is positioned such that the small electrode is the outermost and the large electrode is the innermost feature. When an AC field is induced over the

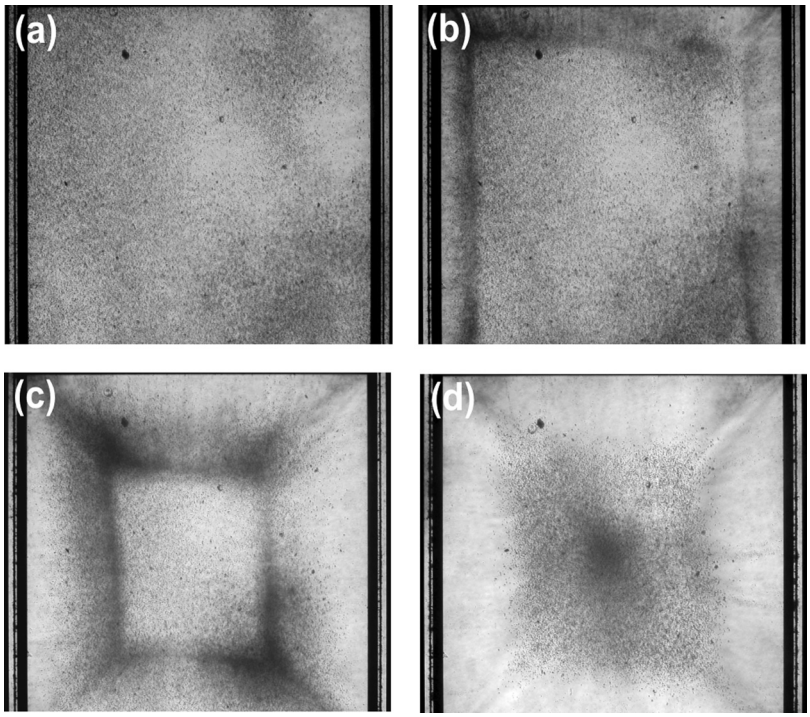

FIG. 2. Micrographs of typical particle collection results for 300 Hz, 800 mV at (a) 0 s, (b) 10 s, (c) 180 s, and (d) 360 s. A line of grouped particles, or particle front, is formed within the first few seconds of applying the AC voltage. The particle front traverses from the edge of the electrodes towards the center of the chip over the course of the trial, forming a rectangular deposit of densely packed particles in the middle of the collection area. The collection patterns are similar to those attained by Bhatt *et al*. (Ref. 26), but thanks to the different principle are attained in 10% of the time.

asymmetric pairs, eddies form over the electrodes.[15,17,27,30,31] These eddies draw the fluid flow directionally from the small electrode towards the large electrode (Figure 1(d)).

The characterization of the planar electrode particle collection system was performed by systematically varying the system parameters. Overall, the highest concentration of particles in the collection area was observed when a denser line of particles, or particle front, was formed within the first few seconds of applying the AC current (Figure 2). The particle front traversed towards the center of the chip, similarly to the on-chip collection device by Bhatt *et al*.,[26] but at much faster rate. Note that the velocities reported here are not the bulk fluid flow velocities as reported in previous ACEO pumping literature,[17–24] but are the rate of motion of the particle front.

A major goal of this study was the determination of the design and operation parameters affecting particle collection efficiency. Rapid detection is required in most lab-on-a-chip devices; thus, we established a target collection time of <15 min. Our strategy for collecting particles was to establish an electrode configuration and operation that induces a bulk, unidirectional ACEO flow toward the center of the corral, then to tune other device design parameters to increase particle collection efficiency. The AC potential was varied from 50 mV to 6 V, while the frequency was varied from 10 Hz to 1 MHz. We discuss the parameters that effect ACEO bulk fluid flow generation in DI water (electrode and gap width) and 1 μm latex particle collection rate (chamber height, applied potential/frequency, electrode repeat segments, electrode geometry, and toggling between optimal DEP and ACEO settings). Lastly, we discuss the effect of changing analyte composition and its relation to the design parameters.

A. Bulk fluid flow generation

1. Electrode and gap width

Electrode asymmetry, imposed by varying electrode width and spacing or introducing roughness to the surface, is what drives ACEO flow in one direction just above the electrode

TABLE I. Electrode design configurations and dimensions (in μm).

Configuration	Small electrode	Small gap	Large electrode	Large gap
1	5	5	30	15
2	5	25	30	75
3	5	5	50	15

surface.[15,30,31] The spacing between electrodes as well as the electrode width is crucial to drive bulk unidirectional ACEO pumping and to induce positive and negative DEP. The size of these eddies above the electrodes is dependent on the AC field gradient and is, therefore, affected by the size of the electrode and the distance between them.[30,31] Previous ACEO pumping devices using asymmetric electrodes have identified 300 Hz, 800 mV as favorable parameters for inducing bulk ACEO flow.[17,18] Thus, the ACEO fluid flows and their efficiency for particle collection for three electrode pattern designs were first evaluated at 300 Hz, 800 mV (Table I).

For each design, some degree of fluid flow was apparent. When an AC was applied to configuration 1, a particle front quickly formed at the edge of the innermost large electrode and proceeded towards the center of the array for approximately 6 min. The particles collected at the center in a well packed structure as desired (Figure 2(d)). For configuration 2, both the large and small gap sizes were increased 5-fold. Rapid particle movement between the electrodes was observed, indicating intensive fluid flow above them. However, no particle front formed at the electrode edge and no particle collection ensued. Similar results were obtained by increasing the width of the large electrode by 66% in configuration 3.

Observations by reflectance and fluorescence microscopy revealed that the particles were being drawn towards and trapped over the large electrodes for both designs 2 and 3. Typically, particle trapping and chaining in the gap between the electrodes is evidence of dielectrophoresis;[14,32,33] however, at this electrode length scale and for 1 μm latex in DI water, 300 Hz, 800 mV was not sufficient to induce DEP. The reason for the collection on the electrodes was that the eddies formed over the electrodes for configuration 2 and 3 were not large enough to drive a bulk fluid flow, so the particles were trapped above the electrodes only. Similar results have been reported using devices with large circular electrode pads over which cells and particles were trapped.[7–11,25] The results are consistent with ACEO pumping models predicting that the optimal pumping widths are 1.5×, 6.55×, and 4.74× for the small electrode, large electrode, and large gap, respectively,[34] so configuration 1, with feature dimensions of 1×, 6×, and 3×, is most effective in generating strong unidirectional fluid velocity.[17,19,23,31,34,35]

B. Particle collection tuning parameters

Once unidirectional ACEO flow is induced by the asymmetric electrodes, the flow pattern must be maintained and directed to a stagnant region over the central collection area. The ACEO flow must also be strong enough to drag the suspended cells or particles from the bulk to the stagnant region. The optimal conditions for the process were established by studying the effect of chamber height, the AC field potential and frequency, number of electrode repeats, electrode geometry and electrode pattern inversion on particle collection to determine the optimal settings for ACEO flow and DEP particle collection. These conditions were then used to demonstrate a combined ACEO/DEP collection technique.

1. Chamber height

It has been reported in the ACEO pumping literature that chamber height has no significant effect on bulk fluid flow or particle motion.[34] While this might be true for delivering a particle from one point to another in a rectangular microfluidic channel, through this study, it was discovered that chamber height is critical when collecting particles in a central stagnant area. We investigated three chamber heights, 250 μm, 750 μm, and 1600 μm using the 5-electrode repeat

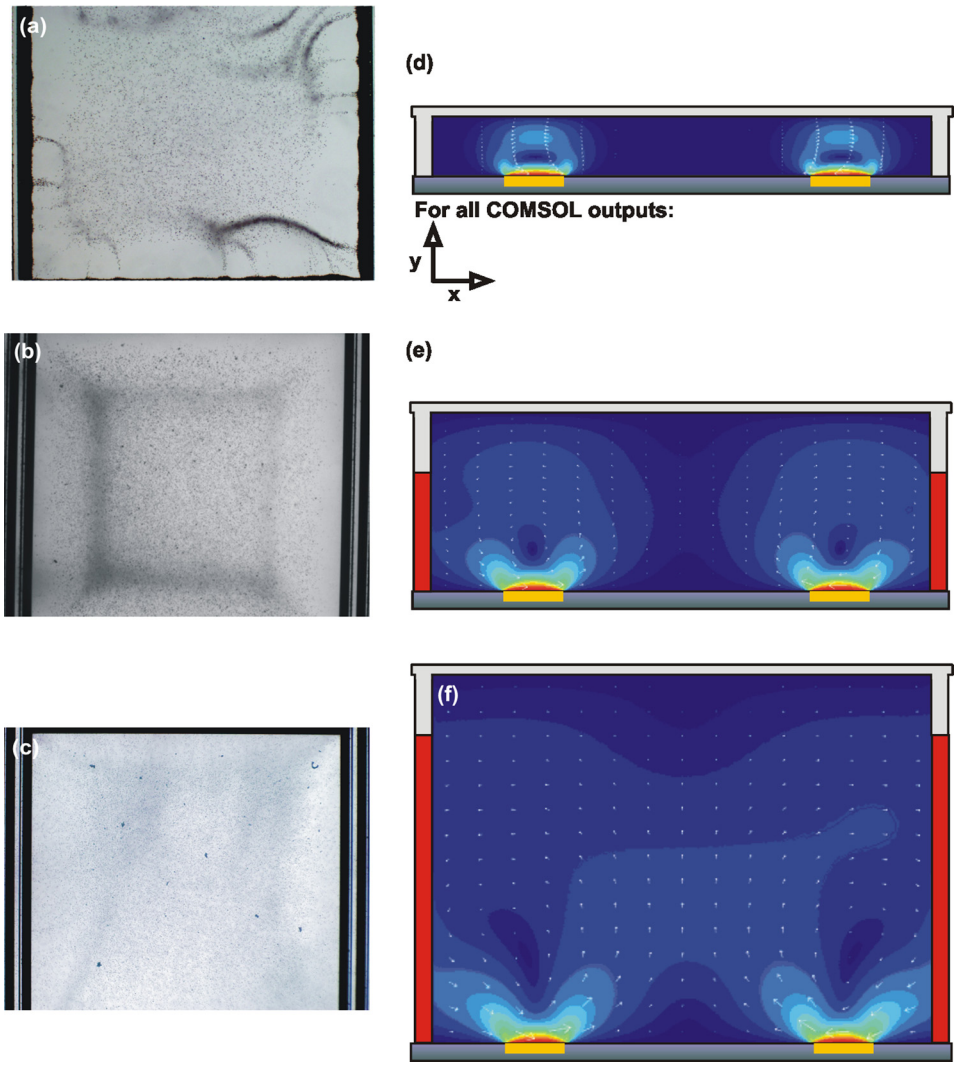

FIG. 3. Effect of chamber height on particle collection. (a)-(c) The top view in real time of particle collection device at varying chamber height. The width of the collection area is 1 mm. (a) At a relatively low height of 250 μm, small rapid eddies form directly over the electrodes and erratic eddies exist along the edge of the chip. Little, if any, particle collection was observed at the center of the collection area. (b) The optimal chamber height is approximately at a 1:0.75 ratio to the width of the collection area on the chip (750 μm). This thickness leads to strong vortices and a well-defined stagnant area the center of the chip. (c) Higher chamber height allows for larger vortices to form over the electrodes, however, these vortices are strong enough to draw the particles away from the electrode chip surface. (d)-(f) Side view of the COMSOL model output for geometry and dimensions corresponding to the particle collection experiments with fluid flow vectors calculated from the fluid dynamics simulations.

configuration (Figure 3). For the 250 μm chamber height, at each investigated AC frequency and potential, eddies were observed to form along the periphery of the collection area at the leading edge of the innermost large electrode (Figure 3(a)). These eddies appeared to have no predictable shape or behavior and to be most turbulent at the corners of the collection area. The particle motion increased as the potential was increased as predicted by previous ACEO asymmetrical electrode pumping studies.[17–23] However, no combination of low potential (250 mV–1 V) or frequency (10 Hz–5 kHz) produced a unidirectional bulk fluid flow that would achieve the desired densely packed formation of particles in the center of the chip.

For the 1600 μm chamber height, a particle front initially formed at the electrode edge within seconds of applying the electric field. The distinct front traversed inward for approximately 1 min, but the particles appeared to be drawn away from the center and upwards into

the chamber. The particles collected at the center were not densely packed (Figure 3(b)). The 750 μm chamber appeared to perform best at all combinations of potentials and frequencies. A particle front clearly formed within a few seconds and traveled towards the center of the collection area (Figure 3(c)). This result was unexpected as the previous ACEO pumping literature reported optimum chamber heights for maximum bulk fluid flow to be approximately half of the length of one electrode repeat segment;[15,31,34] therefore, we expected the 250 μm thick chamber to give us the optimal results for particle collection and bulk fluid flow.

We interpreted these results by simulations using a 2-D fluid dynamics model developed by COMSOL finite element analysis software package. The model examined a side-view cross section of the electrode chip and chamber, bisected across the width of two sides of the equilateral electrode segments. The total electrode segment width and chamber height were analogous to the center collection area and to the dimensions tested experimentally. No-slip boundary conditions were applied at the top of the chamber, the collection area in between the electrode segments, and beyond the outer edge of the electrodes on the glass surface. A linear velocity scaled to the linear particle velocity observed experimentally directly above the electrodes was programmed along the surface of the electrode segments. The relative velocities are depicted by the color schematic in Figures 3(d)–3(f) with red indicating the region of highest velocity. White arrows represent velocity gradient direction. For all chamber heights, bulk circular flow patterns formed, originating at the electrode segments and flowing towards the center of the chip. The no-slip boundary conditions at the center of the chip, chamber top, and at the outer edge of the electrode area give rise to the overall circular motion and the formation of updrafts and downdrafts.

Figures 3(d), 3(e), and 3(f) represent the results for 250 μm, 750 μm, and 1600 μm chamber heights, respectively. In Figure 3(d), at the 1:0.25 collection areas to chamber height scale, the bulk circular fluid flow develops just over the electrode segments. Although there is a distinct stagnant area at the middle, the circular fluid flow does not reach far enough to push particles into the center of the collection area. The particles are most likely drawn into the bulk circular flow and settle along the edges of the small bulk eddies. For chamber heights at a 1:1.6 scale, such as those featured in Figure 3(f), the linear bulk fluid flow is less restricted by the no-slip boundary conditions of the chamber top forming a bulk circular flow pattern with larger diameter. There is a distinct, concentrated stagnant area in the center of the corral and a tangential component of the velocity beyond the electrode segments, which may be responsible for the observed partial collection of particles. Just above the stagnant region in the center of the collection area, however, there is a strong velocity gradient in the y-direction where the bulk circular flow patterns meet. This updraft is likely responsible for the observed partial sweeping of particles away from the collection area.

The 1:0.75 chamber model shown in Figure 3(e) also has a distinct stagnant area at the center of the collection area as in the 1:0.25 and 1:1.6 models. The bulk circular flow patterns originating from the electrodes do not meet in the center to form a distinct updraft, and a strong tangential velocity is present beyond the edge of the electrode segments. The lack of updraft and the strong linear velocity beyond the electrode segment edge are likely responsible for the initial pulse of particles being moved to the center. Without a central updraft, the particles are pushed laterally over the collection area, where they settle and assemble in densely packed formation. This is in agreement with the experimental observation that the 750 μm chamber height offers optimal particle collection. This height was used through the remainder of the study.

2. Potential and frequency

The maximum ACEO pumping velocity requires an optimal potential and frequency.[17–22,24] First, we determined the effect of the potential on our ACEO flow velocity and particle collection efficiency, by varying the applied potential from 50 mV to 800 mV while holding the frequency constant at 300 Hz (the lowest frequency at which ACEO flow was consistently noted). We discuss the effect of increasing frequency later in this section.

Particle motion observations were initiated at an applied potential of 50 mV and increased at 50 mV increments until moving particles were observed just above the electrodes. Time

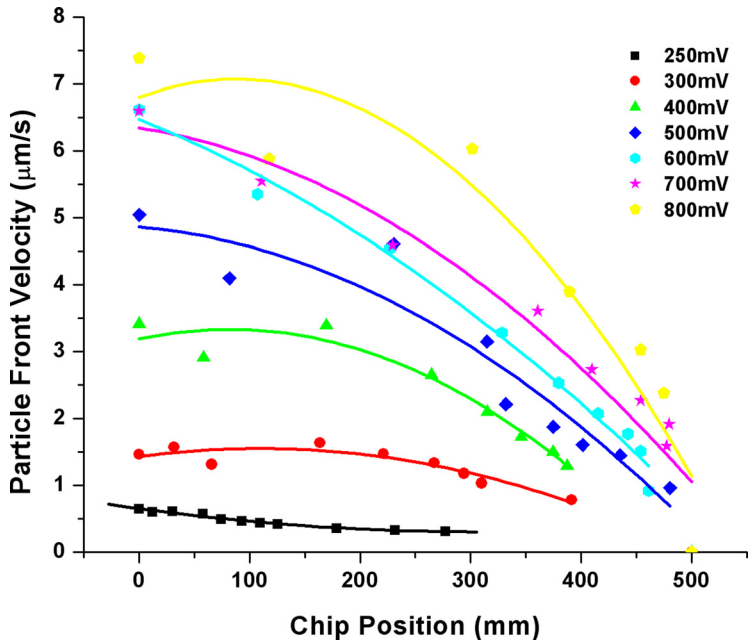

FIG. 4. Particle front velocity at 300 Hz as particles suspended in DI water travel from the electrode edge to the center of the collection area. The electrode edge is at 0, and the center of the chip is at 500 μm. For lower potentials (250–300 mV), the bulk fluid velocity is insufficient to drag the particles to the center of the collection area within the 15 min trials. As potential increases, the bulk fluid velocity increases, drawing the particles to the center.

lapse images of the process were analyzed to calculate particle front velocity and particle collection efficiency. The resulting particle front velocity is graphed against the position on the corral in Figure 4. The particle front velocity is maximal at the electrode edge and decreases as the particle front traverses from the electrode edge towards the center of the collection area. Particle movement was detected at potentials as low as 250 mV; however, the slow front velocity during those trials did not afford sufficient time for the particles to reach the center within 15 min. As the potential increased, the particle front velocity increased as expected. At potentials above 400 mV, the particle front reached the center within the 15 min trial, with the particles reaching the center the fastest (within 6 min) at 800 mV.

The pixel density along the width of the collection area was calculated for applied potentials of 250 mV–800 mV at 280 s, based on the particle velocity analysis. The most rapid, compact collection was achieved at a time of 280 s, which was chosen as the baseline data by which to compare all collection trials. Figure 5 presents a plot of the normalized %DFW (see Sec. II) with respect to collected front position on the chip at 280 s. A negative percentage indicates fewer particles than initially present (e.g., they become swept away by the flow), while a positive percentage indicates accumulated particles. At 300 mV, just above the collection potential threshold, particle movement and some degree of collection are apparent with a negative %DFW (Figure 5). The range of %DFW, however, is between -30% and 30%, indicating very slow particle movement. For 400 mV–600 mV, a distinct particle front could be observed and resulted in a much higher %DFW range of -100% to 75%. The particles are drawn from the electrode edge toward the center but at 280 s, they were maximally concentrated at 350 μm from the edge, short of the center of the collection region.

At 700 mV, we observed more densely packed particles and, thereby, obtained a positive %DFW value in the middle of the collection area. The particles at the perimeter of the 1 mm^2 corral at $t = 0$ reached the stagnant region within 220 s. At longer times, more particles outside the bounds of the electrode corral are drawn into the center. The 60% DFW peak at 500 μm results from the initial collection of particles, while the second peak at 250 μm represents the particles drawn from outside the corral after the electrodes are energized. The outermost

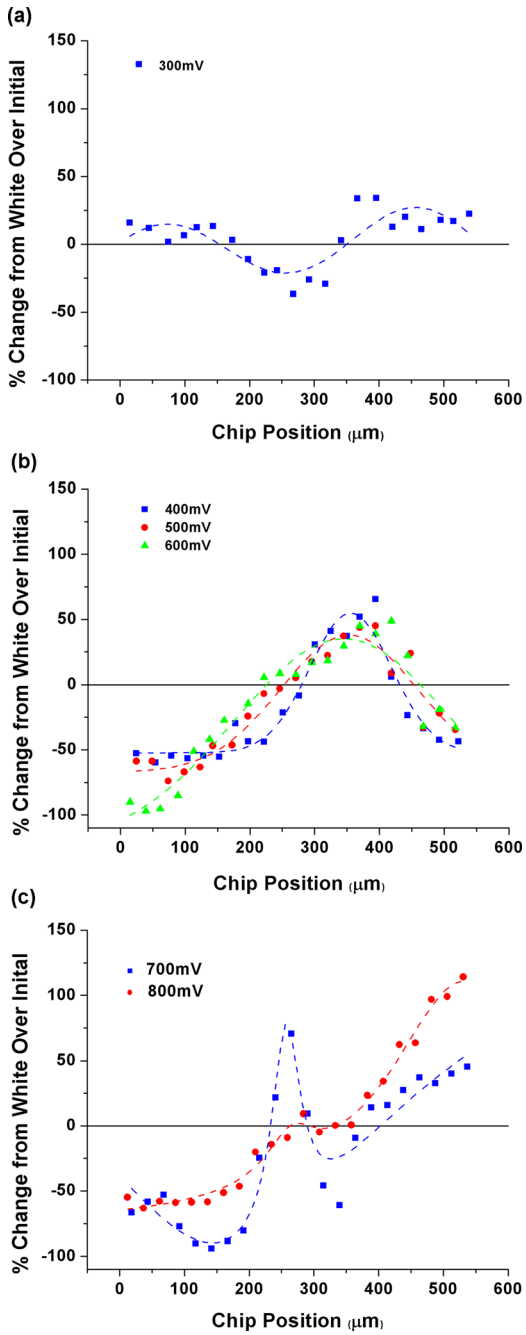

FIG. 5. Pixel density analysis of ACEO particle collection in DI water at 300 Hz, (a) 300 mV, (b) 400–600 mV, and (c) 700–800 mV after 280 s of field application in terms of percent deviation from the initial average pixel color value. The solid points are the experimental data, while the dashed line is its trend. (a) At 300 mV, very little particle movement and a small slow particle front was observed, resulting in little change in the particle density throughout the collection area. (b) From 400 mV to 600 mV, a faster moving, more distinct, particle front was observed, but it was not rapid enough to reach the collection area center. (c) At 700 mV to 800 mV, the efficient collection of particles at the center was confirmed by a positive %DFW.

particles get collected in the corral center in 280 s. At 800 mV, the %DFW exhibited the largest observed variance from −75% to 125% and a maximum % DFW was measured at the collection area center. Potentials above 1 V did not appear to collect particles as densely as 800 mV. The higher flow rate and resulting collection pattern resemble that of the 1600 μm

chamber height (Figure 3) as an upward directed flow drives particles away from the collection area. Therefore, 800 mV was selected as the base potential for subsequent parameter optimization.

An increase in the applied AC potential results in an increase in the magnitude of the electric field, thereby increasing ACEO flow rate.[17–22,24] However, its effect on the particle collection process is much more complex, given the interplay of fluid flow, viscous drag, velocity gradients, and particle sedimentation. Thus, it is possible to tune the particle collection front velocity, the density of the collection, and the collection time by altering the applied potential, while the most efficient process does not necessarily occur at the fastest ACEO flow rate.

The particle movement induced by frequencies of 300 Hz, 1 kHz, and 2.5 kHz was measured at potentials ranging from 250 mV to 800 mV. At frequencies approaching zero, the capacitance of the electric double layer impedes the ionic flows necessary to induce ACEO flow. As the frequency increases, the electron flow through the circuit happens rapidly enough to overcome the electric double layer capacitance and induce the flow.[14] For our device, ACEO flow appeared to begin above 100 Hz and dissipated after 2.5 kHz, similarly to the data of Brown *et al*. with latex suspensions in $NaNO_3$ solutions.[17] The particle front velocity for each frequency increased as expected when the potential was increased. Little difference in the particle front velocity was detectable between 300 Hz and 1 kHz. These findings are in general agreement with earlier ACEO data below 3 V, where optimums were observed between 500 Hz and 5 kHz with little change in the flow velocity.[17,18,21] However, when the frequency was increased above 1 kHz, fewer particles were collected in the center of the corral than at lower frequencies (Figure 6). Inspection of the electrode gaps under higher magnification revealed that the particles were being drawn between the smaller gaps in gold electrodes and forming chains by DEP. Particle chaining occurred more rapidly at frequencies above 2.5 kHz. DEP became the predominant effect at frequencies above 10 kHz. DEP trapping and chaining between the electrode pairs impeded ACEO particle collection in the center, however, were able to combine ACEO and DEP in a synergistic manner as described in Subsection B 5 below.

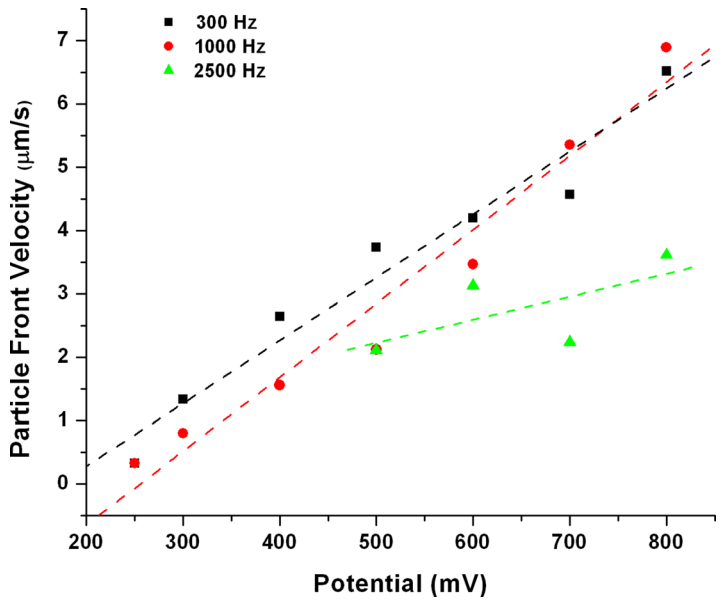

FIG. 6. Particle front velocity analysis in the low-frequency regime at 800 mV. DI water suspensions require low potentials and frequencies to induce ACEO bulk fluid flow. Very little change in the particle front velocity is observed for small frequency changes between 300 Hz and 1 kHz. As the frequency was raised above 2.5 kHz, DEP was observed, reducing the amount of particles in the collection area and reducing the apparent particle front velocity.

3. Number of electrode repeats

The particle collection performance of the electrode chip design was further characterized by changing the number of asymmetric electrode pairs surrounding the collection corral. According to the model proposed by Ramos *et al.*,[27] a large vortex forms over the large electrode at the edge adjacent to the small gap drawing the fluid towards and across the electrode. The two vortices formed over the small electrode are rapid, but are in opposite directions and have little influence over the bulk fluid flow velocity. For chamber heights greater than the width of the electrode repeat segments, the fluid will flow in the direction from the small electrode to the large one.[27,34] Therefore, each electrode pair generates one large vortex that drives the overall fluid flow. As the number of electrode repeats increase, the number of driving vortices and the linear velocity above the electrodes also increase. We observed the particle collection processes at 300 Hz, 800 mV for electrode chips containing 1, 3, 5, and 10 electrode repeats over 15 min. As expected, devices with 1 and 3 electrode repeats exhibited slower particle collection than chips with 5 electrode pairs. Neither chip design induced a particle front capable of drawing particles to the center of the collection area. One electrode repeat is sufficient to draw the particles just beyond the large electrode as indicated by the %DFW (see Figure S1 in Supplementary Material[29]), which becomes slightly positive at the electrode edge, but remains unchanged towards the center of the collection area. In the 3-electrode pair repeat device, a faint particle front formed initially and slowly traversed approximately 250 μm towards the center of the collection area (Figure 7(d)).

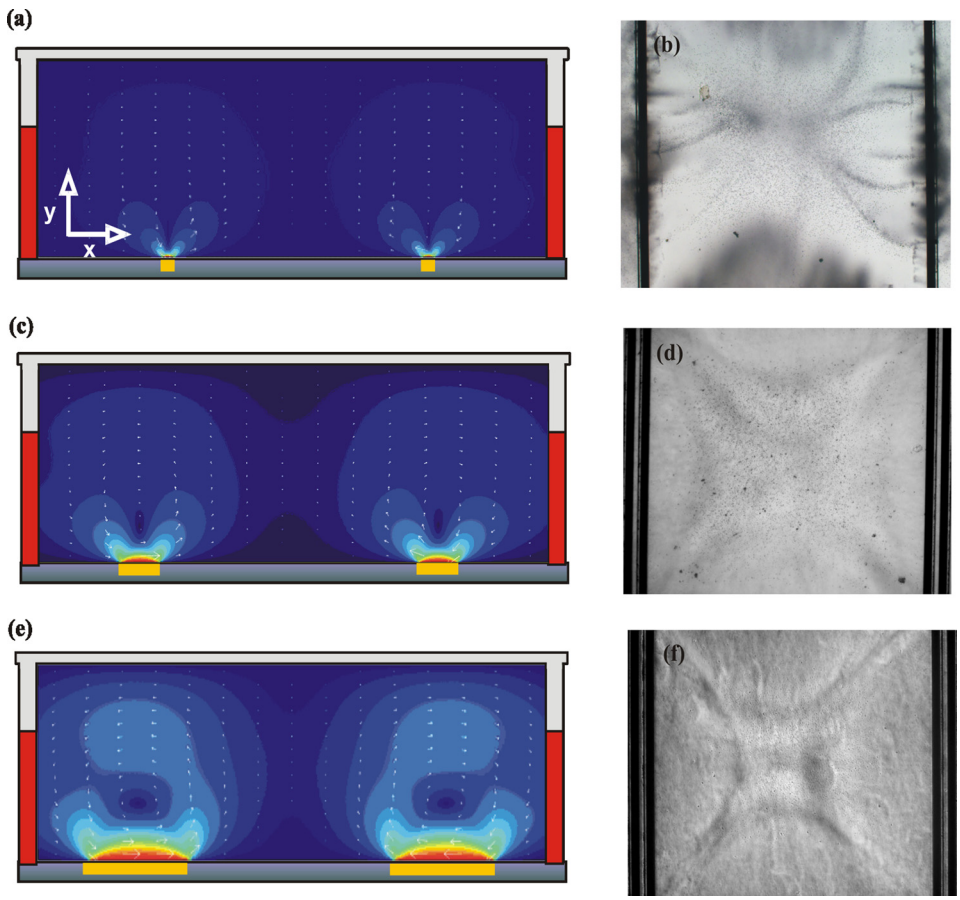

FIG. 7. COMSOL finite element analysis models and micrographs taken at 280 s for increasing number of electrode pattern repeats: one (a),(b), three (c),(d), and ten (e),(f). (a), (c), (e) are the side view of COMSOL simulation outputs and (b), (d), (f) are the top view of experimental micrographs. The width of the experimental collection area is 1 mm. The bulk fluid flow eddies formed as a result of ACEO increase in size and velocity as the number of repeats increases. None of the repeat designs resulted in densely packed collection of particles as in the five repeat design [Figures 3(b) and 3(e) and Table II in the Supplementary Material (Ref. 29)].

The 10-electrode repeat device behaves like that of the 5-repeat device; upon field application, a dark, distinct particle front was formed immediately upon application of the AC field and was drawn towards the center of the chip. After approximately 100 s, the center of the chip began to lighten, indicating that particles were being drawn away from the collection area. At 280 s, a −60% DFW at the chip center indicated fewer particles are in the center of the collection area than initially present. Thus, the 10-repeat does not effectively collect 1 μm particles under these conditions, though preliminary observations suggest the configuration might be useful for larger particles, surface treated electrodes, or higher electrolyte concentrations.

A fluid dynamics model of the electrode repeat microfluidic chambers was developed in COMSOL to interpret these results. No-slip boundary conditions in the x-direction were implemented at the chamber top and to either side of the electrode sets. A linear velocity was programmed just above the electrodes for a length proportional to that of the total width of the electrode pair segments (Figures 7(a), 7(c), and 7(e)). For the 1-repeat system, a small eddy develops just over the electrodes, but the flow in the x-direction is dissipated just beyond the electrode edge. The eddies over the electrodes are more pronounced in the 3- and 5-repeat designs. In the simulation for the 10-repeat design, the x-direction fluid velocity is much higher than that of the 5-repeat design, but a strong y-direction flow in the middle of the chip where the eddies meet is likely responsible for drawing particles into the bulk fluid flow eddy.

The simulations are in good correlation to the experimental data. Similarly to the dependence on applied potential, the optimal particle collection occurs for a linear velocity over the electrode segments creating circular bulk eddies that do not meet above the collection center. Overall, the number of electrode repeats and the applied potential both play a major role in inducing linear flow in the devices. Although the characterization was only performed for 1 μm particles, the linear velocity can be adjusted to optimize collection of larger and smaller particles and cells.

4. Electrode geometry

In this cycle of experiments, we compared the efficiencies of the chip design with rectangular corral with chips having circular electrode pattern. The diameter of the circular collection area was made large enough to fit the 1×1 mm^2 detection area in the center ($d = 1.414$ mm). Circular electrode pairs with 1, 3, 5, and 10 repeats were energized by an AC voltage of 800 mV, 300 Hz. The ACEO flow on each of the circular repeat pairs acted similarly to their rectangular counterparts. In the 1-repeat circular pattern device, small eddy lines formed along the electrode edge similar to those observed on the rectangular design; however, no localized areas of particle collection developed near the electrode edge and the % DFW varied very little. With 3-repeat segments, a distinct particle front was formed at the electrode edge that propagated towards the center of the chip over 15 min. This particle front did not reach the center, exhibited nearly identical behavior to that of the rectangular design and did not disappear until approximately 600 s. The 10-repeat design immediately produced a distinct particle front, visibly drawing particles towards the center. However, after 120 s, the particles were already drawn away from the surface of the collection area by a bulk updraft fluid flow, similar to the one seen with rectangular electrodes (Figure 5). The % DFW at 280 s indicates a small band of particle deposits beginning 150 μm from the electrodes. The 5-repeat design induced the optimal x-direction fluid velocity to draw the most particles to the center of the collection area (Figure 8(c)). The %DFW range is significantly smaller than that of the rectangular design; however, the area under the 5-repeat circle curve is 1.5 times larger than that of the 5-repeat rectangular curve (Figure 8(a)).

The collection patterns result from the flow pattern and dynamics established by the electrode "pumps". In the rectangular design, the quadrilateral unidirectional flows impinge along the diagonals of the collection area, resulting in a discernable diamond-like shape in the particle front and collection patterns. The flow generated in a radial pattern over the circular electrode chip uniformly converges at the center of the collection area. It may appear that the circular electrode pattern is the better candidate for optimal particle collection, but each design has

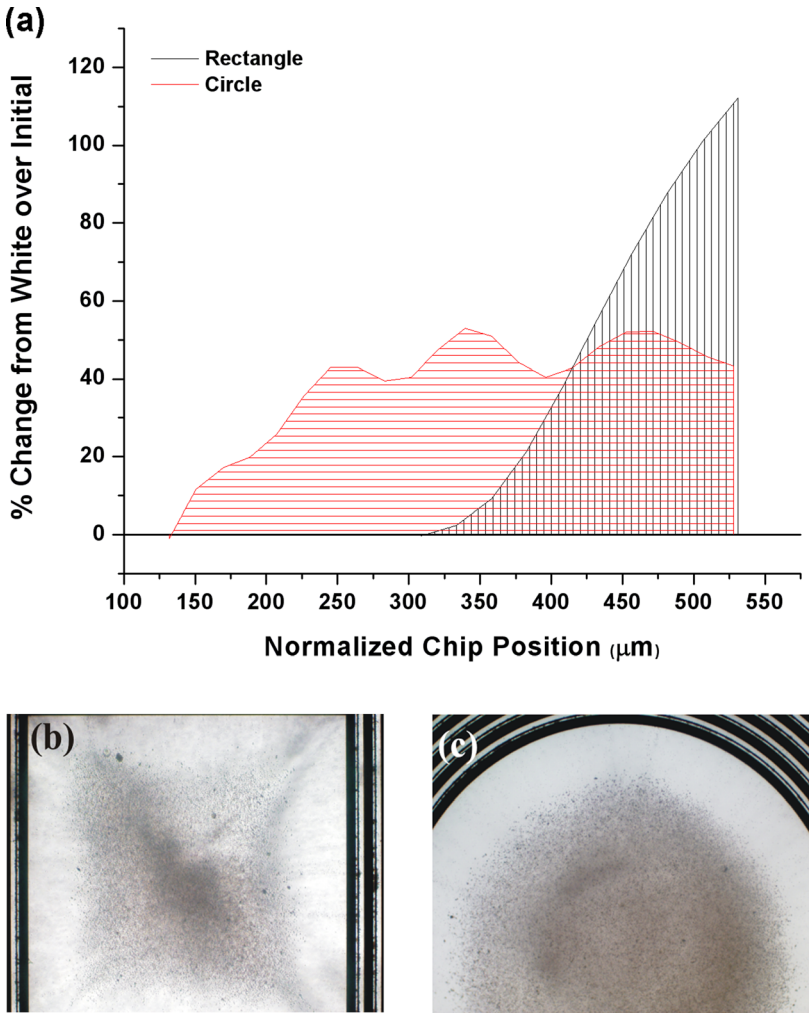

FIG. 8. Micrographs and pixel analysis for circle geometry electrode segment repeat trials at 300 Hz, 800 mV. The %DFW analysis indicates similar results to the rectangular electrode geometry in that an optimum x-direction fluid velocity is needed to form a densely packed bed of particles in the center of the collection area. The 5-repeat design appeared to induce the optimum fluid velocity to draw 1 μm particles to the collection center. Despite the lower %DFW range than in the rectangular case, (a) integrating the area under the %DFW curves for both the rectangular and circular geometries indicates the circular geometry is capable of drawing a larger amount of particles into the collection area. This is further seen by comparing the micrographs of the (b) 5-repeat rectangular design and (c) 5-repeat circular design results at 280 s.

specific application-dependent advantages. The rectangular design is optimal for collecting particles in a concise, small area of the collection center, while the circular design is better for collecting a larger number of particles in a uniform deposit over the entire corral surface.

5. Synergistically combining DEP and ACEO Regimes

After observing DEP effects in DI water suspensions of latex particles at frequencies above 1 kHz and optimal ACEO particle collection at 800 mV and 300 Hz, we evaluated the joint use of both DEP and ACEO effects to improve the ACEO-driven particle collection observed at 800 mV and 300 Hz. The goal was to use DEP for rapid trapping of the particles in the gaps and then push the collected particles in the corral by ACEO. The potential was fixed at 800 mV, while the frequency was toggled between 300 and 5000 Hz at varying intervals of time. For each trial, the particles were collected by DEP at 5 kHz for a period of time ranging from 5 to 40 s, followed by ACEO driven collection in the center of the chip for an additional 5–40 s. The cycle was repeated for a total of 3.5 min. Toggling intervals of 5 s were neither

adequate to collect particles by DEP nor long enough to bring a significant amount of particles to the center of the chip. Increasing the DEP collection time to 30 s appeared to be sufficient to draw particles between the electrodes in the small gaps. For the ACEO interval, it was observed that 10 s fluid motion was sufficient to induce particle motion to the center of the corral. Alternating 30 s DEP intervals and 10 s ACEO intervals resulted in drastically decreased collection times (see Supplementary Material[29]) and an increase in the amount of particles collected as compared to ACEO alone.

C. Effects of medium composition and particle type

1. Electrolyte concentration

Many point-of-care and cell detection devices operate with media of high electrolyte concentrations. In AC electrohydrodynamics, ions in electrolyte solutions reduce double layer thickness and, therefore, suppress ACEO flow.[14] We investigated the ACEO particle collection in dilute PBS (phosphate buffered saline) for applied potentials of 800 mV–2 V and frequencies ranging from 100 Hz to 1 MHz. For concentrations above 0.01 mM PBS, no particle movement was detected at all frequencies and potentials below 1.2 V, the thermodynamic threshold for electrochemical reactions.[36] Above 1.2 V and below frequencies of 100 kHz, bubbles formed on the electrode surface in evidence of undesired faradic reactions at the gold electrodes. Particle motion was observed below 1.2 V for electrolyte suspensions concentrations below 0.01 mM PBS; however, the resulting particle front velocity decreased sharply and particles did not reach the center of the collection area (Figure 9). As with the DI water suspensions, increasing frequency only slightly increased the particle front velocity. To determine if the particle collection device could be used for unmodified environmental water analysis, latex particles were suspended in tap water (conductivity 235 mS/m). The collection pattern observed at 900 mV and 1 kHz was similar to that observed in 0.001 mM PBS. The decrease in pumping velocity in high ionic strength media and undesired faradic reactions has been widely reported in ACEO pumping devices.[17,19,20,22] Our device can be used as designed presently to collect cells and particles in low electrolyte solutions (conductivities below 36.0 μS/cm), but work is in progress to develop electrode surface modifications that could suppress or eliminate the faradic reactions that occur in higher conductivity solutions.

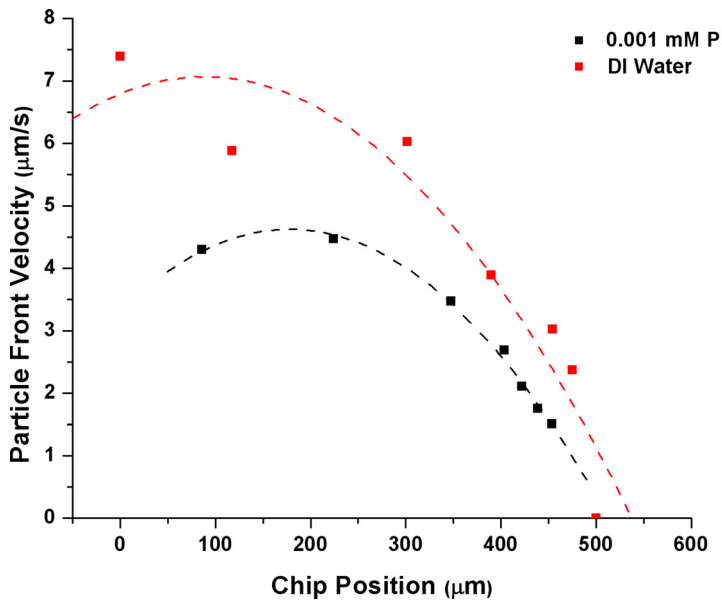

FIG. 9. Particle front velocity for latex particles suspended in DI water and 0.001 mM PBS at 500 Hz, 1 V.

2. Particle size and type

We verified the ability of the device to collect larger latex particles (5 μm) and yeast cells in DI water suspensions. For the 5-repeat electrode device, the applied 800 mV, 300 Hz AC current did induce an ACEO flow, but the velocity was not great enough to carry the particles to the collection area. Increasing the potential to 2 V and the number of repeats from 5 to 10 induced a flow strong enough to carry the larger particles to the collection area. Likewise, the yeast cells having a diameter of approximately 5.0 μm also required 2 V applied potentials and 10-electrode repeats to induce flows great enough to collect the cells in the center of the device. The yeast cells also were prone to adhering to the glass substrate surface outside the electrodes, in between the electrodes, and in the collection area. Overall, the device can reliably collect particles within broad ranges of sizes and types.

IV. CONCLUSIONS

We report the principle of operation and in-depth characterization of a co-planar asymmetric electrode device that induces a simultaneous, quadrilateral unidirectional flow, which is capable of rapid, dense particle collection. The asymmetrical planar electrode design collects the particles suspended in low-electrolyte water over a 1×1 mm collection area at relatively low applied potentials and frequencies. This configuration provides effective operation by using electrodes surrounding the collection area without obscuring the optical sensor that may be paired with the devices. It makes possible the design of collection devices that may be compatible with evanescent wave sensing, grating couplers, ring resonators, and interferometers.

This device is flexible in that design parameters affecting collection time, full flow development, and the x-direction velocity over the electrodes can be tuned so as to be applied to varying suspensions of both particles and cells. The chamber height was observed to affect the flow pattern over the electrodes and into the collection area, and a 1:1 ratio of chamber height to collection area were found to be optimal. Both the applied potential and the number of electrode repeat segments can be increased and decreased to tune collection parameters for varying suspensions of particles and cells. The geometry of the electrode system does not alter the induction of ACEO flow, but can be altered to achieve more uniform deposition of the particles in the center of the device. These tunable parameters and the photolithographic fabrication of the chip enable it to be easily coupled with surface-bound optical detection methods.

The development of such devices needs to overcome one additional issue. High electrolyte suspensions continue to be problematic. As most biological suspension use salt buffer solutions or saline in nature, it is essential to develop collection devices operating in such media. It has been suggested that modifying the electrodes may reduce or eliminate the propensity for the electrochemical reactions to occur.[37,38] For now, we have shown that surface-pattern directed ACEO flow is useful for collecting analytes in tap water suspensions, leading us to believe the device can be used for environmental water applications.

ACKNOWLEDGMENTS

This research was supported by RTI International, Research Triangle Park, NC and a NIRT grant from the US National Science Foundation (No. CBET-0609087).

[1]S. Gupta, S. Huda, P. K. Kilpatrick, and O. D. Velev, Anal. Chem. **79**, 3810 (2007).
[2]L. Yang and R. Bashir, Biotechnol. Adv. **26**, 135 (2008).
[3]V. Berry, A. Gole, S. Kundu, C. J. Murphy, and R. F. Saraf, J. Am. Chem. Soc. **127**, 17600 (2005).
[4]M. Varshney and Y. B. Li, Biosens. Bioelectron. **22**, 2408 (2007).
[5]J. Suehiro, A. Ohtsubo, T. Hatano, and M. Hara, Sens. Actuators B **119**, 319 (2006).
[6]S. Grego, J. R. McDaniel, and B. R. Stoner, Sens. Actuators B **131**, 347 (2008).
[7]K. F. Hoettges, M. B. McDonnell, and M. P. Hughes, J. Phys. D **36**, L101 (2003).
[8]K. F. Hoettges, M. P. Hughes, A. Cotton, N. A. E. Hopkins, and M. B. McDonnell, IEEE Eng. Med. Biol. Mag. **22**, 68 (2003).
[9]R. Krishnan, B. D. Sullivan, R. L. Mifflin, S. C. Esener, and M. J. Heller, Electrophoresis **29**, 1765 (2008).
[10]R. Krishnan and M. J. Heller, J. Biophotonics **2**, 253 (2009).

[11]R. Krishnan, D. A. Dehlinger, G. J. Gemmen, R. L. Mifflin, S. C. Esener, and M. J. Heller, Electrochem. Commun. **11**, 1661 (2009).
[12]D. Hou, S. Maheshwari, and H. C. Chang, Biomicrofluidics **1**, 13 (2007).
[13]M. Felten, W. Staroske, M. S. Jaeger, P. Schwille, and C. Duschi, Electrophoresis **29**, 2987 (2008).
[14]H. Morgan and N. G. Green, *AC Electrokinetics: Colloids and Nanoparticles*, 1st ed. (Research Studies Press Ltd., Williston, VT, USA, 2003).
[15]A. Ajdari, Phys. Rev. E **61**, R45 (2000).
[16]A. Gonzalez, A. Ramos, N. G. Green, A. Castellanos, and H. Morgan, Phys. Rev. E **61**, 4019 (2000).
[17]A. B. D. Brown, C. G. Smith, and A. R. Rennie, Phys. Rev. E **63**, 016305 (2001).
[18]V. Studer, A. Pepin, Y. Chen, and A. Ajdari, Microelectron. Eng. **61–62**, 915 (2002).
[19]V. Studer, A. Pepin, Y. Chen, and A. Ajdari, Analyst **129**, 944 (2004).
[20]J. P. Urbanski, J. A. Levitan, D. N. Burch, T. Thorson, and M. Z. Banzant, J. Colloid Interface Sci. **309**, 332 (2007).
[21]W. Hilber, B. Weiss, M. Mikolasek, R. Holly, K. Hingerl, and B. Jakoby, J. Micromech. Microeng. **18**, 064016 (2008).
[22]M. Bligh, K. G. Stanley, T. Hubbard, and M. Kujath, J. Micromech. Microeng. **18**, 055007 (2008).
[23]M. Mpholo, C. G. Smith, and A. B. D. Brown, Sens. Actuators B **92**, 262 (2003).
[24]M. Lian and J. Wu, Appl. Phys. Lett. **94**, 064101 (2009).
[25]P. K. Wong, T. H. Wang, J. H. Deval, and C. M. Ho, IEEE/ASME Trans. Mechatron. **9**, 366 (2004).
[26]K. H. Bhatt, S. Grego, and O. D. Velev, Langmuir **21**, 6603 (2005).
[27]A. Ramos, A. Gonzalez, A. Castellanos, N. G. Green, and H. Morgan, Phys. Rev. E **67**, 056302 (2003).
[28]S. Grego, A. Huffman, M. Lueck, B. R. Stoner, and J. Lannon, Microelectron. Eng. **87**, 1846 (2010).
[29]See supplementary material at http://dx.doi.org/10.1063/1.3620419 for electrode design considerations, effect of number of electrode repeats, effect of flow inversion on particle collection.
[30]M. Z. Bazant and Y. X. Ben, Lab Chip **6**, 1455 (2006).
[31]P. Garcia-Sanchez, A. Ramos, N. G. Green, and H. Morgan, IEEE Trans. Dielectr. Electr. Insul. **13**, 670 (2006).
[32]S. Gupta, R. G. Alargova, P. K. Kilpatrick, and O. D. Velev, Soft Matter **4**, 726 (2008).
[33]S. Gupta, R. G. Alargova, P. K. Kilpatrick, and O. D. Velev, Langmuir **26**, 3441 (2010).
[34]L. H. Olesen, H. Bruus, and A. Ajdari, Phys. Rev. E **73**, 056313 (2006).
[35]S. Debesset, C. J. Hayden, C. Dalton, J. C. T. Eijkel, and A. Manz, Lab Chip **4**, 396 (2004).
[36]A. J. Bard and L. R. Faulkner, *Electrochemical Methods: Fundamentals and Applications* (John Wiley & Sons, Inc., Hoboken, NJ, USA, 2001).
[37]M. Z. Bazant and T. M. Squires, Curr. Opin. Colloid Interface Sci. **15**, 203 (2010).
[38]J. Cheng, E. L. Sheldon, L. Wu, A. Uribe, L. O. Gerrue, J. Carrino, M. J. Heller, and J. P. O'Connell, Nat. Biotechnol. **16**, 541 (1998).